Supporting information

Hydrogen radical pathway for efficacious electrochemical nitrate reduction to ammonia over Fe-polyoxometalate/Cu electrocatalyst

Heebin Lee[1,‡], Keon-Han Kim[2,‡], Reshma R. Rao[3], Dong Gyu Park[1], Won Ho Choi[4], Jong Hui Choi[1], Dong Won Kim[1], Do Hwan Jung[1], Ifan E. L. Stephens[3], James R. Durrant[5,], and Jeung Ku Kang[1,*]*

[1]Department of Materials Science and Engineering and NanoCentury Institute, Korea Advanced Institute of Science and Technology (KAIST), 291 Daehak-ro, Yuseong-gu, Daejeon 34141, Republic of Korea

[2]Chemical Science Division, Lawrence Berkeley National Laboratory, 1 Cyclotron Road, Berkeley, CA 94720, United States of America

[3]Department of Materials, Imperial College London, London W12 0BZ, United Kingdom

[4]Department of Petrochemical Materials, Chonnam National University, 50 Daehak-ro, Yeosu-si 59631, Republic of Korea

[5]Department of Chemistry and Centre for Processable Electronics, Imperial College London, London W12 0BZ, United Kingdom

[‡] Contributed equally to this work.

[*]Corresponding authors: j.durrant@imperial.ac.uk, jeungku@kaist.ac.kr

Methods

Materials. $Na_2WO_4 \cdot 2H_2O$ (Sigma Aldrich, ACS reagent, ≥99%), H_3PO_4 (Junsei, 85%), NaCl (Sigma Aldrich, ACS reagent, ≥99%), KCl (Sigma Aldrich, ACS reagent, ≥99%), $FeCl_2 \cdot 4H_2O$ (Sigma Aldrich, ReagentPlus, 98%), LiCl (Sigma Aldrich, ACS reagent, ≥99%), HCl (Duksan chemical, 35-37wt%), Methanol (Sigma Aldrich, HPLC Plus, ≥99.9%), Nafion perfluorinated resin solution (Sigma Aldrich, 5 wt% in mixture of lower aliphatic alcohols and water, contains 45% water), KOH (Sigma Aldrich, ACS reagent, ≥85%), $K^{14}NO_3$ (Sigma Aldrich, ACS reagent, ≥99%), $K^{15}NO_3$ (Sigma Aldrich, 98 atom% ^{15}N).

Synthesis of Preyssler anion ($K_{12.5}Na_{1.5}[NaP_5W_{30}O_{110}] \cdot 15H_2O$). Preyssler anion was prepared via the hydrothermal method. 9.90 g (27 mmol) of $Na_2WO_4 \cdot 2H_2O$ and 1.17 g of NaCl were dissolved in 9 ml of deionized (DI) water and 7.0 ml of 85% H_3PO_4 solution. The encapsulated autoclave was placed in the convection oven (Heratherm OMS60, Thermoscientific) and suffered heat treatment under 398 K for 20 hours. After cooling by room temperature, 3.00 g (40 mmol) of KCl was added to the as-prepared solution under vigorous stirring for 30 min. The pale-yellow precipitate was obtained by filtration and recrystallized with 10 ml of 353 K deionized water. The final recrystallized precipitate was collected by filtration and dried in the vacuum oven.

Precipitation of Fe-polyoxometalate. Fe-polyoxometalate was synthesized with the as-prepared Preyssler anion and metal precursor. 130 mg (0.657 mmol) of $FeCl_2 \cdot 4H_2O$, 130 mg (0.015 mmol) of $K_{12.5}Na_{1.5}[NaP_5W_{30}O_{110}] \cdot 15H_2O$ and 0.2967 g (7 mmol) of LiCl were added to 7 ml of deionized water (pH 1, adjusted by HCl). The solution was put into the 25 ml round bottom flask with a reflux condenser and heated at 363 K for 20 hours under vigorous stirring. After heating, the solution was transferred to a glass vial and solvent evaporation proceeded under 353 K until the total volume of solution reaches ~1 ml. The glass vial containing solution was placed into a sealed 120 ml flask with 20 ml of MeOH and MeOH vapor facilitated the crystallization of Fe-polyoxometalate. Dark brown crystals appeared in a few days and were collected by filtration after two weeks. Resulting crystals were rinsed by MeOH several times to remove excess salts.

Electrode preparation. First of all, Cu metal foam (1 cm x 2 cm) was cleansed by acetone for 20 minutes and 3 M HCl solution for 1 hour under sonication, in order. The catalyst solution was prepared with the followed ratio; 1 mg of catalyst:5 μl of Nafion perfluorinated resin solution:100 μl of EtOH. 100 μl of the catalyst solution was dropped on the as-cleansed Cu metal foam and dried the electrode in the ambient atmosphere. The preparation of the electrode was completed by the dropping and drying processes twice. For the spectroelectrochemical measurements, Fe-POM/Cu catalyst was deposited on an FTO substrate. First, Cu was deposited on a clean FTO substrate through sputter deposition. Next, a thin layer of Ti (~5 nm) was sputtered on the FTO substrate with the

depositing rate of 0.0806 nm/s to ensure the Cu sticks to the substrate. Copper films (thickness of ~50 nm) were then deposited from a metallic Cu target with the depositing rate of 0.0138 nm/s. The same catalyst ink and loading condition were used to attach Fe-POM on Cu-deposited FTO.

Characterization. The X-ray diffraction patterns (XRD) were obtained by the SmartLab diffractometer (RIGAKU, D/MAX-2500) using Cu-Kα radiation operating condition of 40 kV and 30 mA. The chemical states of materials were measured by the X-ray photoelectron spectroscopy (XPS) (Thermo VG Scientific, K-Alpha). The morphology of photoanode was obtained by the field emission-scanning electron microscope (FE-SEM; JEOL, JSM-7600F) and transmission electron microscopy (TEM; JEOL, JEM-ARM200F). The Fourier transform-infrared (FT-IR) spectra were collected with the FT-IR-6100 (JASCO) with a range of 400 − 4000 cm^{-1}. The electron paramagnetic resonance (EPR) spectra were obtained by the electron spin resonance (ESR) spectrometer (JEOL, JES-FA200) with the following parameters: microwave power = 9.48 GHz; modulation amplitude = 0.2 G; modulation frequency = 100 kHz; non-saturated microwave power = 9 mW; temperature = 298 K. Additionally, the X-ray absorption fine structure (XAFS) measurements using the X-ray absorption near edge structure (XANES) and extended X-ray absorption fine structure (EXAFS) analyses were conducted in a 7D beam line at Pohang Accelerating Laboratory (PAL, Republic of Korea), where a calibration of Fe K-edge spectrum was accomplished by employing the reference spectrum from the corresponding Co foil. The light absorption spectra were measured by the ultraviolet−Visible spectroscopy (JASCO V-570 spectrometer) under the air and room temperature condition. The water vapor adsorption analysis performed using a BELSORP-max gas adsorption analyzer (Microtrac MRB corp.). All samples were measured at 298K after evacuating at 373K for 24h. The ^{1}H-NMR spectra were obtained by Bruker Avence Neo 600 (600 MHz).

Electrochemical measurement. The three-electrode H-type electrochemical cell separated by Nafion perfluorinated membrane was used to measure electrochemical properties. Pt coil and Hg/HgO (in 1 M KOH solution) electrodes were used as counter and reference electrodes, respectively. 1 M KOH electrolyte solutions with various concentration of KNO_3 were used for verifying the electrochemical yield of ammonia. The linear sweep voltammetry (LSV) was carried out from open circuit voltage to -1.35 V vs Hg/HgO with the sweep rate of 10 mV/s. The electrochemical impedance spectra (EIS) were recorded at direct current (dc) potential of -0.2 V vs RHE and an alternating current (ac) potential frequency range of 100000 − 0.1 Hz with an amplitude of 10 mV. Electrochemically active surface area was measured by cyclic voltammetry with various scan rate of 20, 40, 60, 80 and 100 mV/s in voltage region without peak current.

Quantification of molecules. Ammonia production was quantified by the modified indophenol blue method. 0.2

mL of electrolyte was adopted and diluted to 2 mL with deionized water after electrochemical reaction. Then, 2 mL of 2 M NaOH solution containing 5 wt% sodium citrate and 5 wt% salicylic acid was added to diluted ammonia containing electrolyte. Then, we put 1 mL of 0.05 M NaClO and 0.2 mL of 1 wt% $C_5FeN_6Na_2O$ solution. The mixed solution was kept in dark container until the solution color changed completely. The concentration of ammonia is proportional to the absorbance at a wavelength of 655 nm, which was measured by the ultraviolet-visible (UV-vis) spectrometer. The relationship between ammonia concentration and absorbance at 655 nm was calibrated with different concentrations of ammonium chloride solutions, as shown in Supplementary Fig. S3. The NO_2^- concentration was quantified by dissolving paminobenzenesulfonamide (20 g) and N-(1-naphthyl) ethylenediamine dihydrochloride (1 g) into the mixture of DI water (250 mL) and phosphoric acid (50 mL). Then, this solution was diluted to 500 mL of volume, and subsequently mixed with electrolyte from the cathodic counterpart. Finally, NO_2^- can be detected at 540 nm of wavelength using the ultraviolet-visible absorption spectroscopy. The NO_3^- concentration was determined by mixing 1 M HCl (0.2 mL) and 0.8 wt% sulfamic acid solution (0.02 mL) before adding to the NO_3 solution (10 mL). The absorption intensities at wavelengths of 220 and 275 nm were measured and calculated by the following equation of '$A = A_{220nm} - 2A_{275nm}$.' A GC-MS (Agilent, GC-7890A and MS-5975C) equipped with a capillary column (Supleco, 30 m 0.32 mm) and MSD (Mass selective detector, inert triple-axis detector) were utilized for gas phase product detection. To quantify the $^{14}NH_4^+$ using ^1H NMR (600 MHz) measurements, a series of $^{14}NH_4Cl$ solutions with defined concentrations (1, 2, 5 and 10) were prepared as standards. A 125 µl of the standard solution/electrolytes was mixed with 125 µl of 15 mM maleic acid in DMSO-D_6 (99.9 atom% D), 50 µl of 4 M H_2SO_4 in DMSO-D_6 and 750 µl of DMSO-D_6. The peak area integral ratio of $^{14}NH_4^+$ to maleic acid is positively correlated with the $^{14}NH_4^+$ concentration.

***Operando* spectroelectrochemical analysis.** Spectroelectrochemical measurements were made on the samples deposited on FTO substrate. Measurements were conducted in a three-electrode cell using a home-built spectroscopy setup. The potential was measured with respected to an Ag/AgCl reference electrode (saturated KCl). The reference electrode was calibrated versus the reversible hydrogen electrode. A Pt mesh was used as the counter electrode. For the light source, a stabilized 10mW tungsten-halogen from Thorlabs (SLS201L) was used with a collimating add on (SLS201C). The light emitted from the lamp was transmitted through the sample and collected using a 1 cm diameter liquid light guide (Edmund optics). The transmitted light to the spectrograph was first collimated and refocused using two 5 cm planoconvex lenses (Edmund) in order to optimally match the optical components of the spectroscope (Kymera 193i, Andor), CCD camera (iDus Du420A-BEX2-DD, Andor). In order to ensure high signal to noise ratio, the detector was maintained at -80^{0}C during the measurements. An Ivium Vertex potentiostat was used. A custom-built LabView software was used for data acquisition. In order to obtain

spectral changes as a function of potential, measurements were conducted in potentiostatic mode. At each potential, the equilibration time was 1 second, before the optical spectra was measured. For each potential, 30 averages of the spectra were taken, before moving to the next potential. The current was also measured at the same time using the potentiostat.

Supporting figures and tables

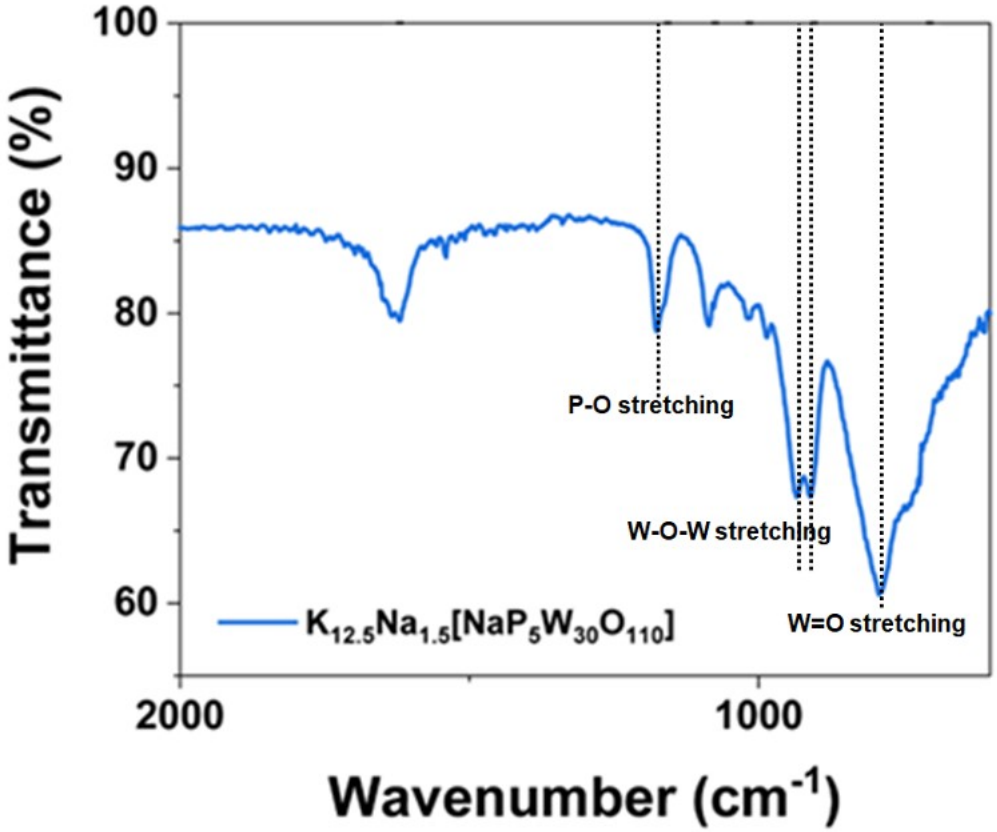

Figure S1. Fourier transformed infrared (FT-IR) spectroscopy of Preyssler anion ($[NaP_5W_{30}O_{110}]^{14-}$).

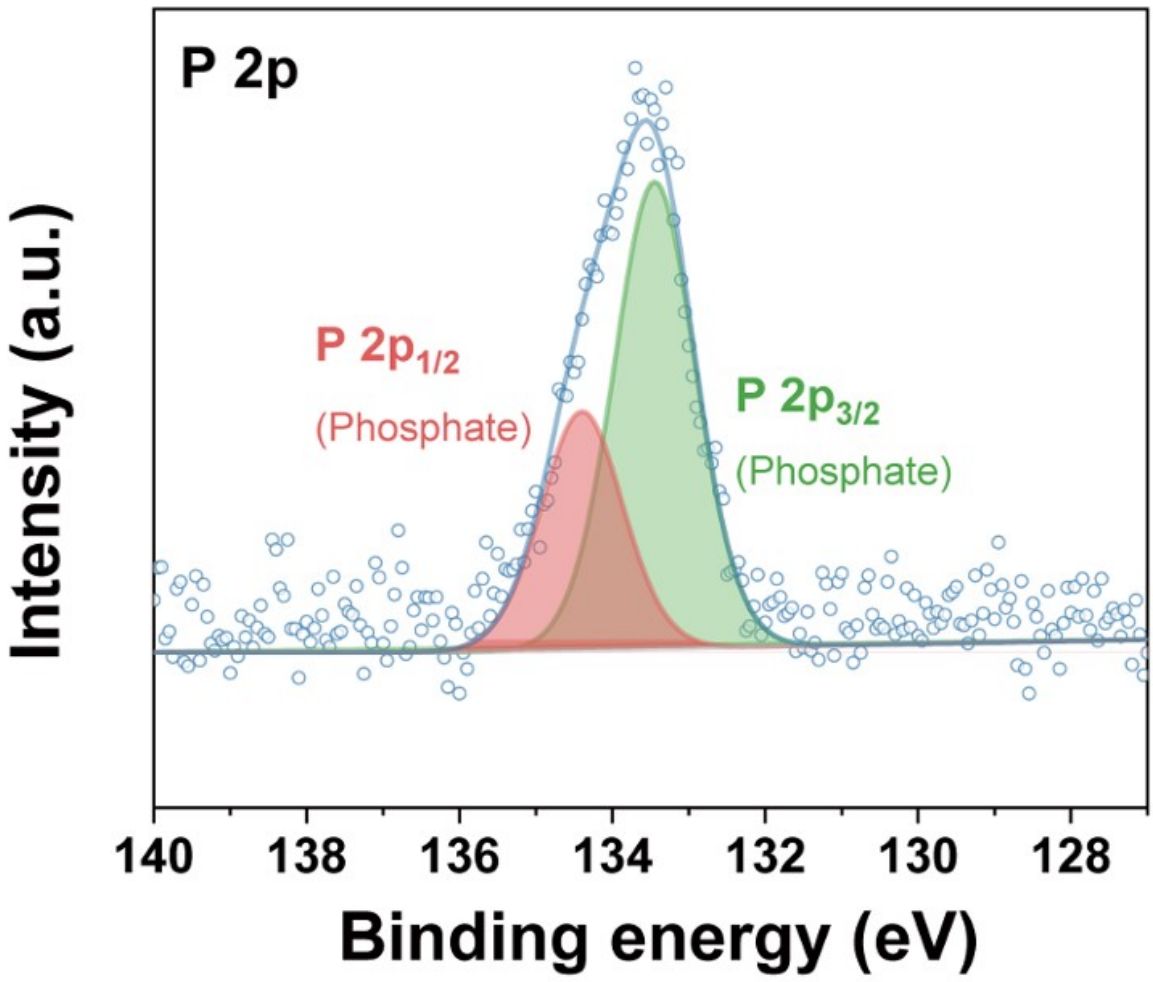

Figure S2. X-ray photoelectron spectroscopy (XPS) P 2p scan for Fe-POM.

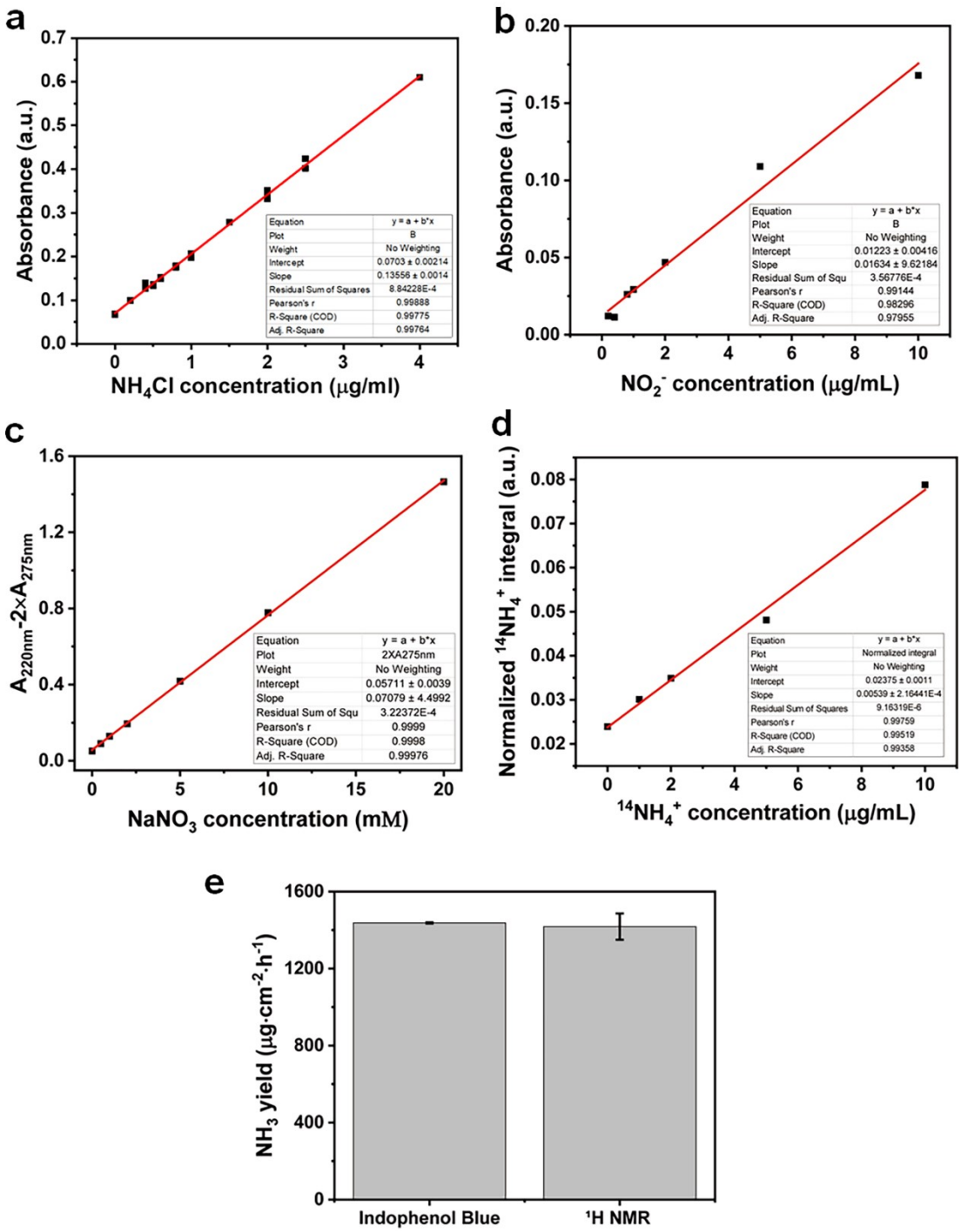

Figure S3. Electrochemical performances as a function of concentration of nitrate used. Relationships (a) between optical absorbance at the wavelength of 660 nm and NH_4Cl concentration (measured by the indophenol blue method), (b) between optical absorbance at the wavelength of 540 nm and $NaNO_2$ concentration, and (c) between A_{220nm}-2×A_{275nm} equation and $NaNO_3$ concentration. (d) Calibration curve for $^{14}NH_4^+$ concentration using ^{1}H NMR, where $^{14}NH_4^+$ peak area integrals were normalized to that of maleic acid. (e) Comparison of the ammonia yield rate over Fe-POM/Cu hybrid electrocatalyst quantified by the Indophenol blue titration and ^{1}H NMR. The electrolysis was carried out at -0.2 V vs. RHE for one hour in 1 M KOH with 500 ppm NO_3^-.

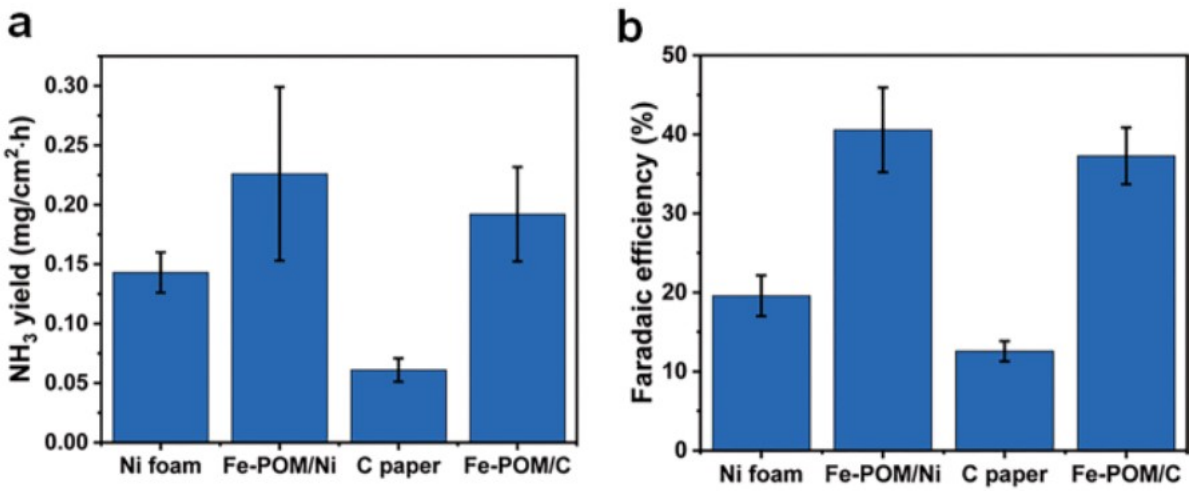

Figure S4. Electrochemical NO_3^- reduction using Ni metal foam and carbon paper with or without Fe-POM . (a) NH_3 yields and (b) faradaic efficiencies using Ni foam and C paper with or without Fe-POM at -0.2 V vs RHE in 1 M KOH + 500 ppm KNO_3.

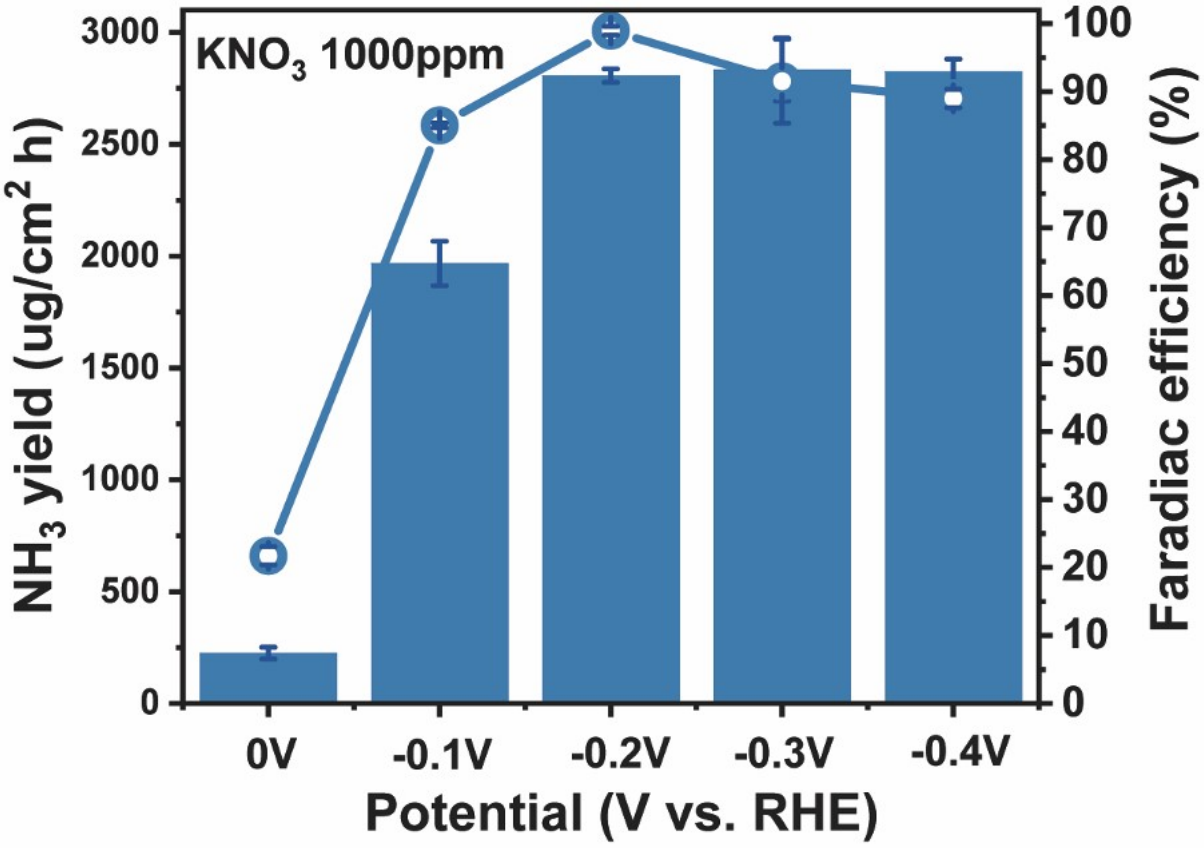

Figure S5. NH_3 yields and faradaic efficiencies with various applied potentials of Fe-POM/Cu electrode in 1 M KOH + 1000 ppm KNO_3.

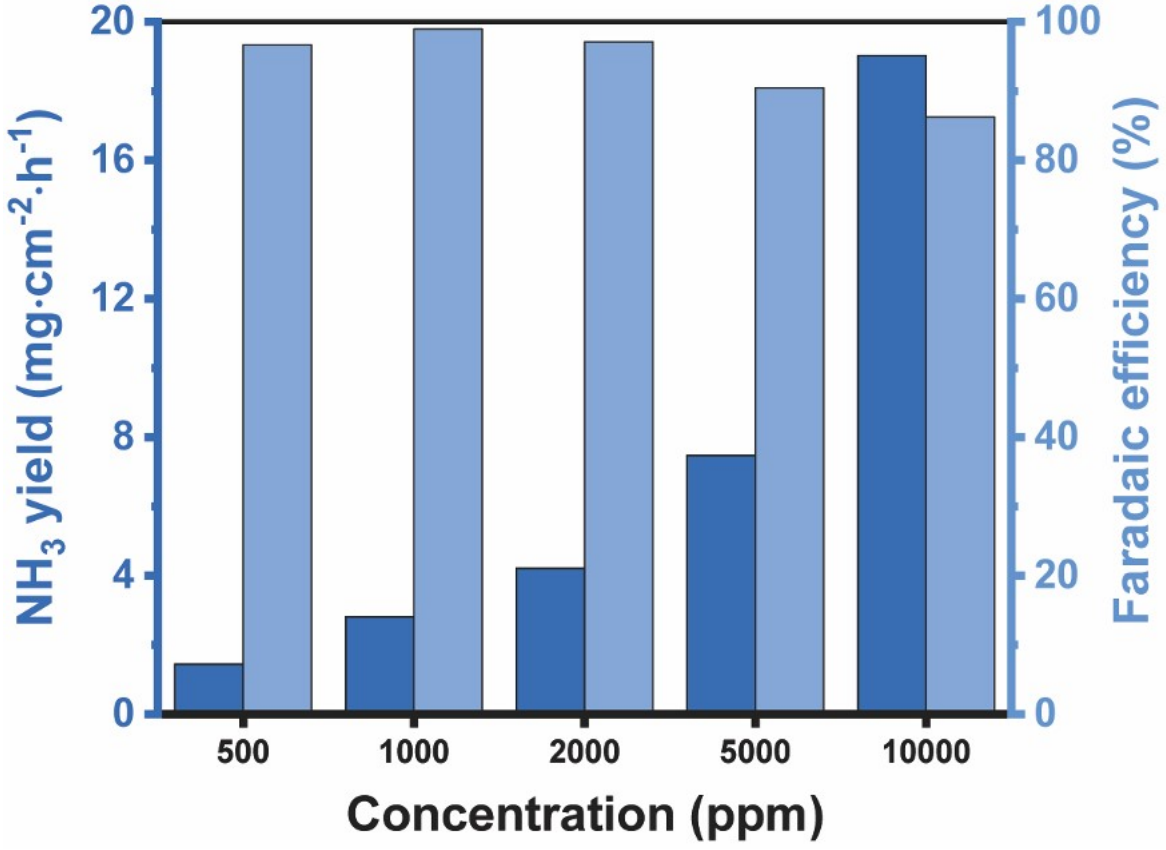

Figure S6. NH_3 yields and faradaic efficiencies of Fe-POM/Cu electrode in highly concentrated nitrate solution with 1 M KOH at -0.2 V vs RHE for an hour.

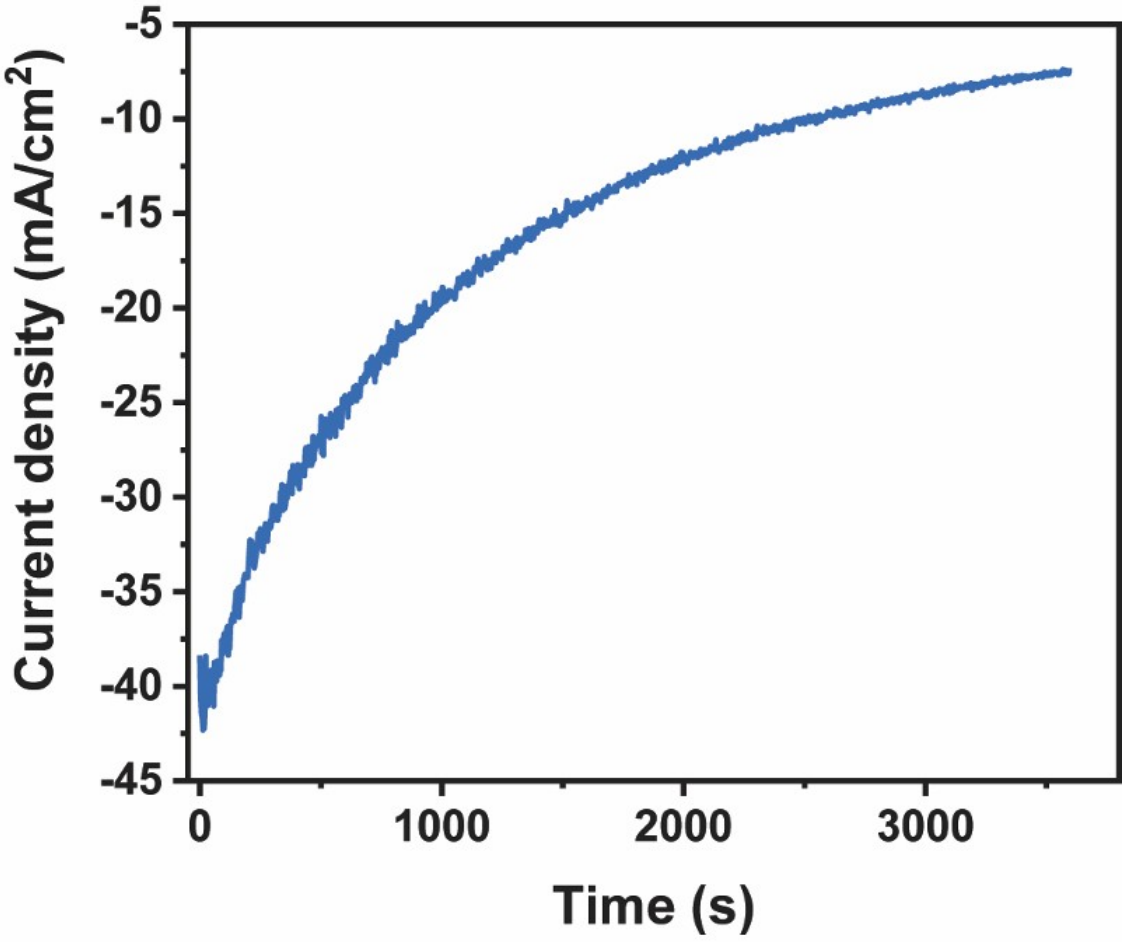

Figure S7. Chronoamperometric curve at 0.2 V vs RHE of Fe-POM/Cu electrode in 1 M KOH + 500 ppm KNO_3.

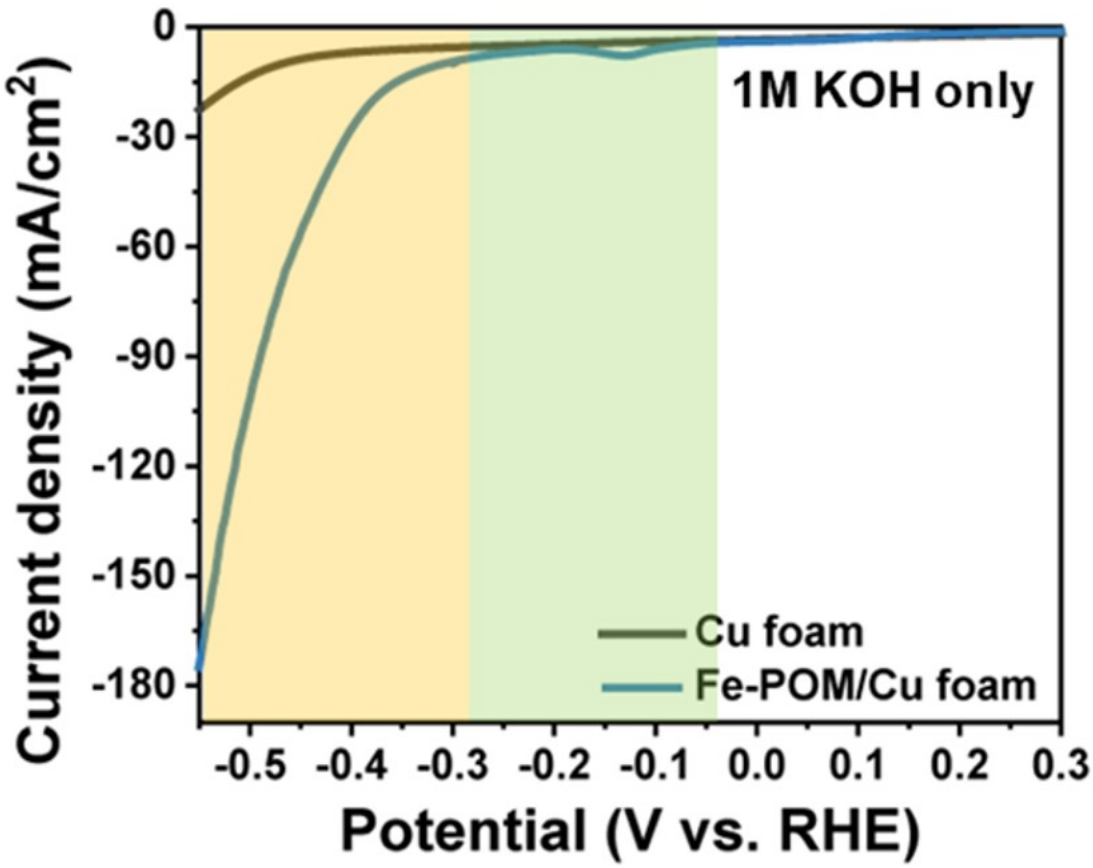

Figure S8. Linear sweep voltammetry (LSV) plots of bare Cu foam and Fe-POM attached Cu foam in 1M KOH electrolyte.

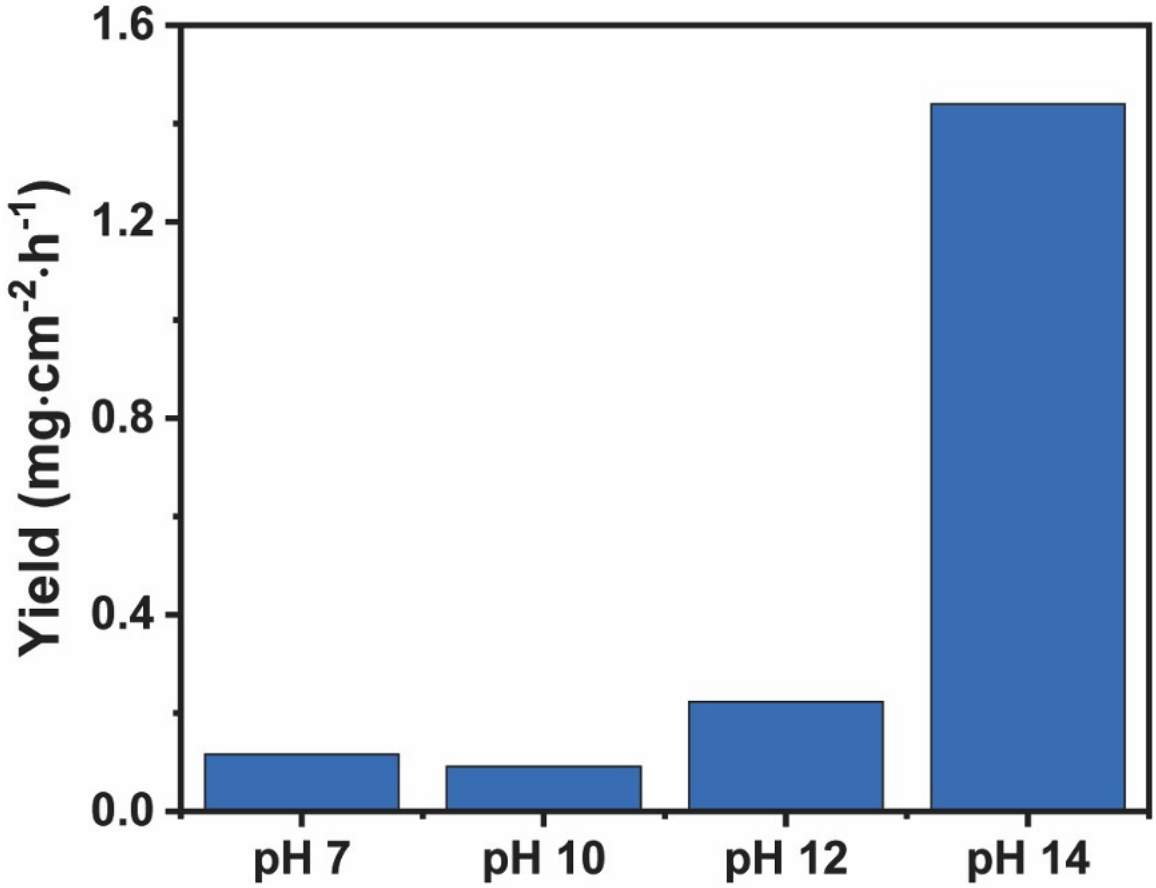

Figure S9. NH_3 yield of Fe-POM/Cu electrode depending on different pH values at -0.2 V vs RHE for an hour in 500 ppm KNO_3 solution.

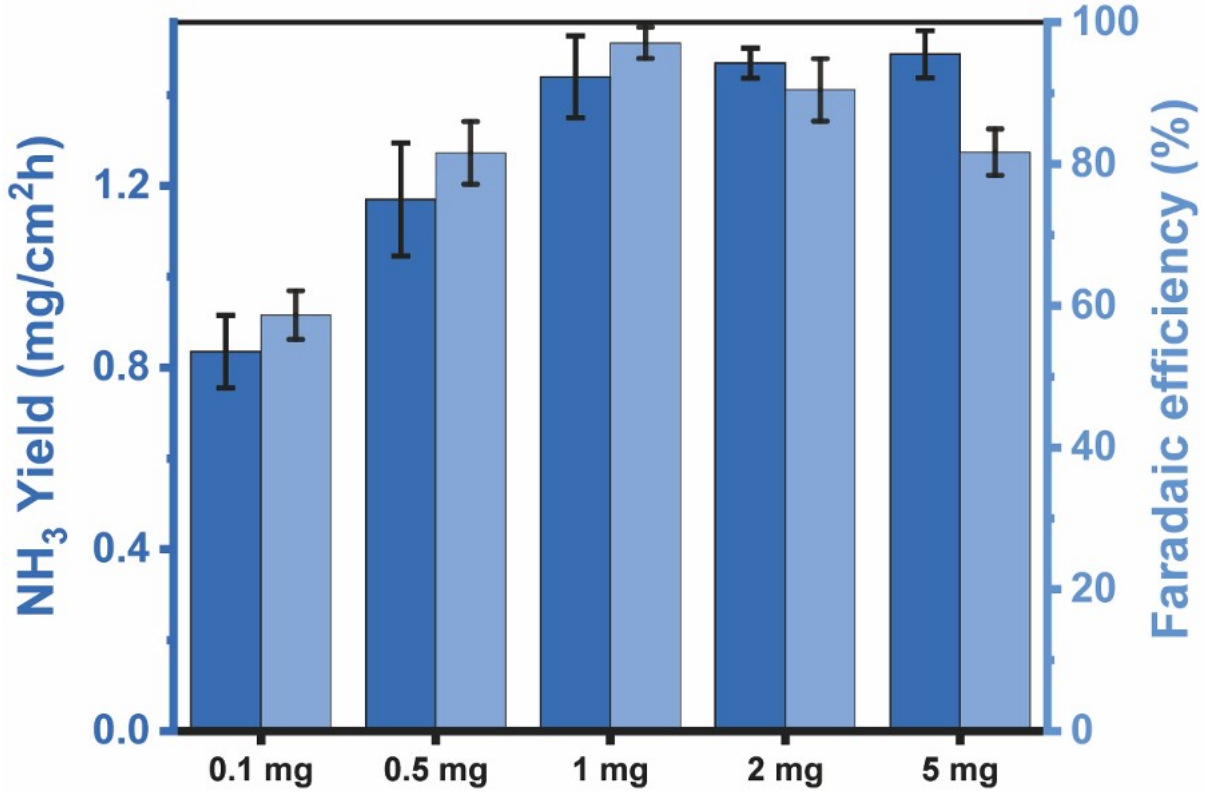

Figure S10. NH_3 yield and FE of Fe-POM/Cu electrode depending on the loading amount of Fe-POM per square centimetre at -0.2 V vs RHE in 1 M KOH + 500 ppm KNO_3.

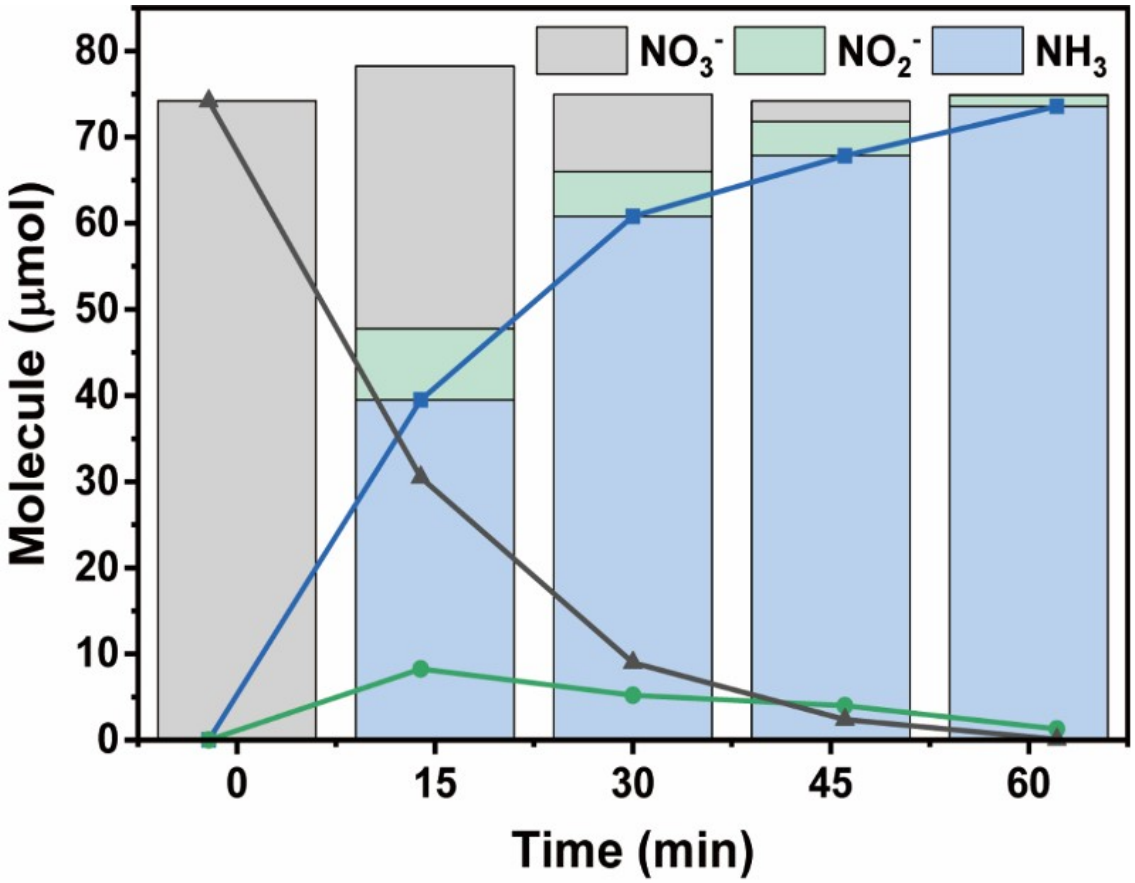

Figure S11. Time-dependent product variation analysis of Fe-POM/Cu at -0.2 V vs RHE in 1 M KOH + 500 ppm KNO_3

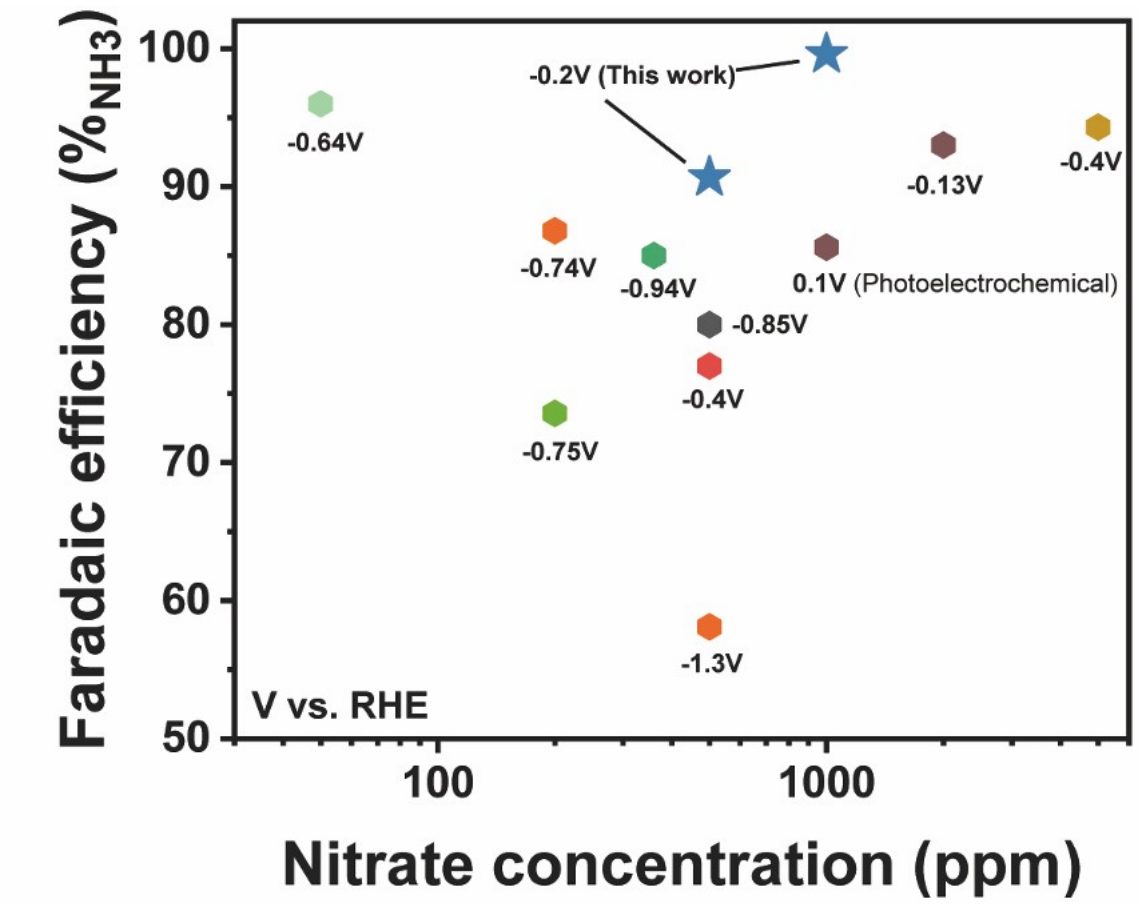

Figure S12. Performances for nitrate reduction to ammonia using various different materials.

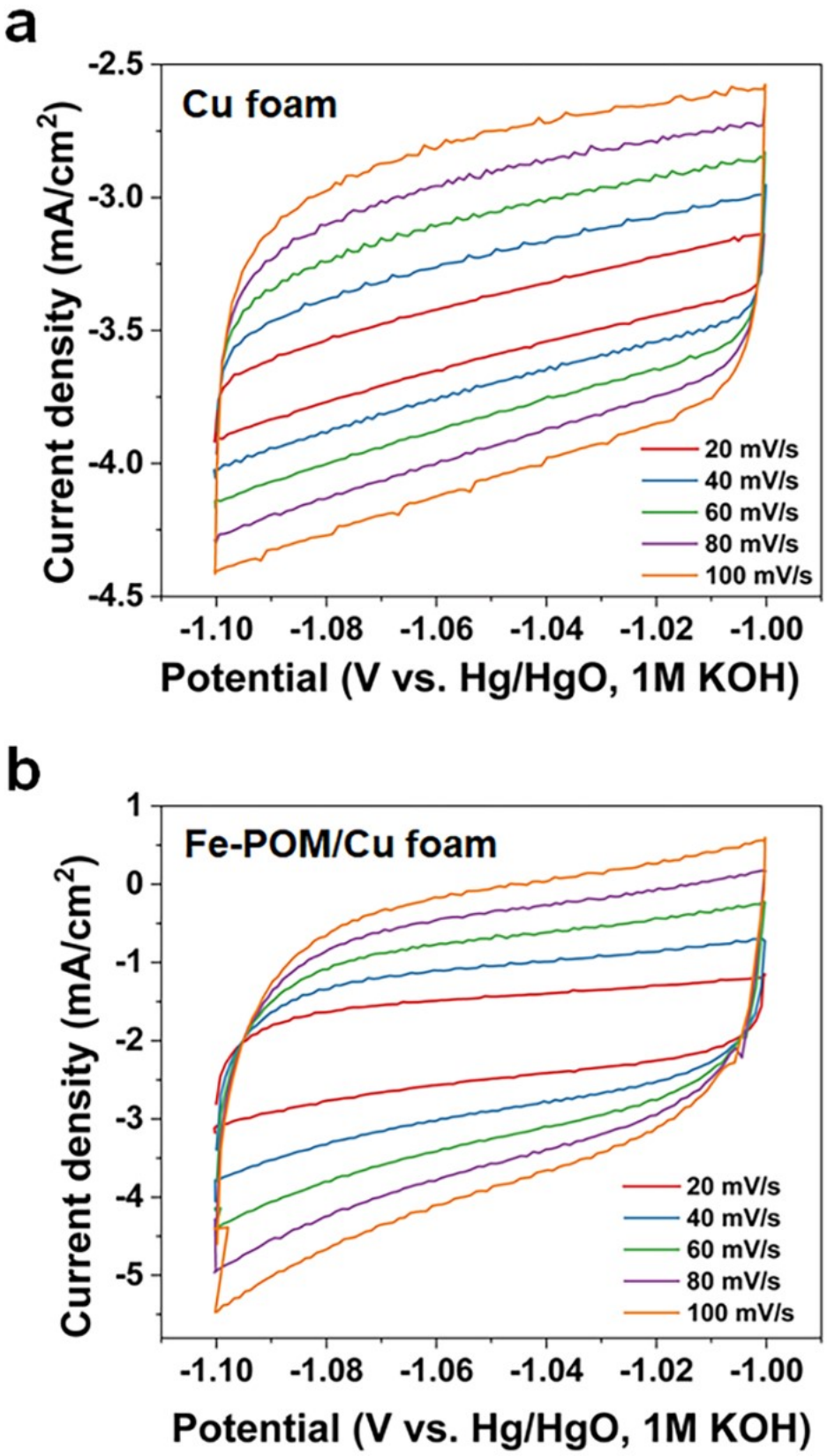

Figure S13. Cyclic voltammetry (CV) plots. Those for (a) bare Cu foam and (b) Fe-POM attached Cu foam with various scan rates of 20, 40, 60, 80 and 100 mV/s, where 1M KOH solution was used as an electrolyte.

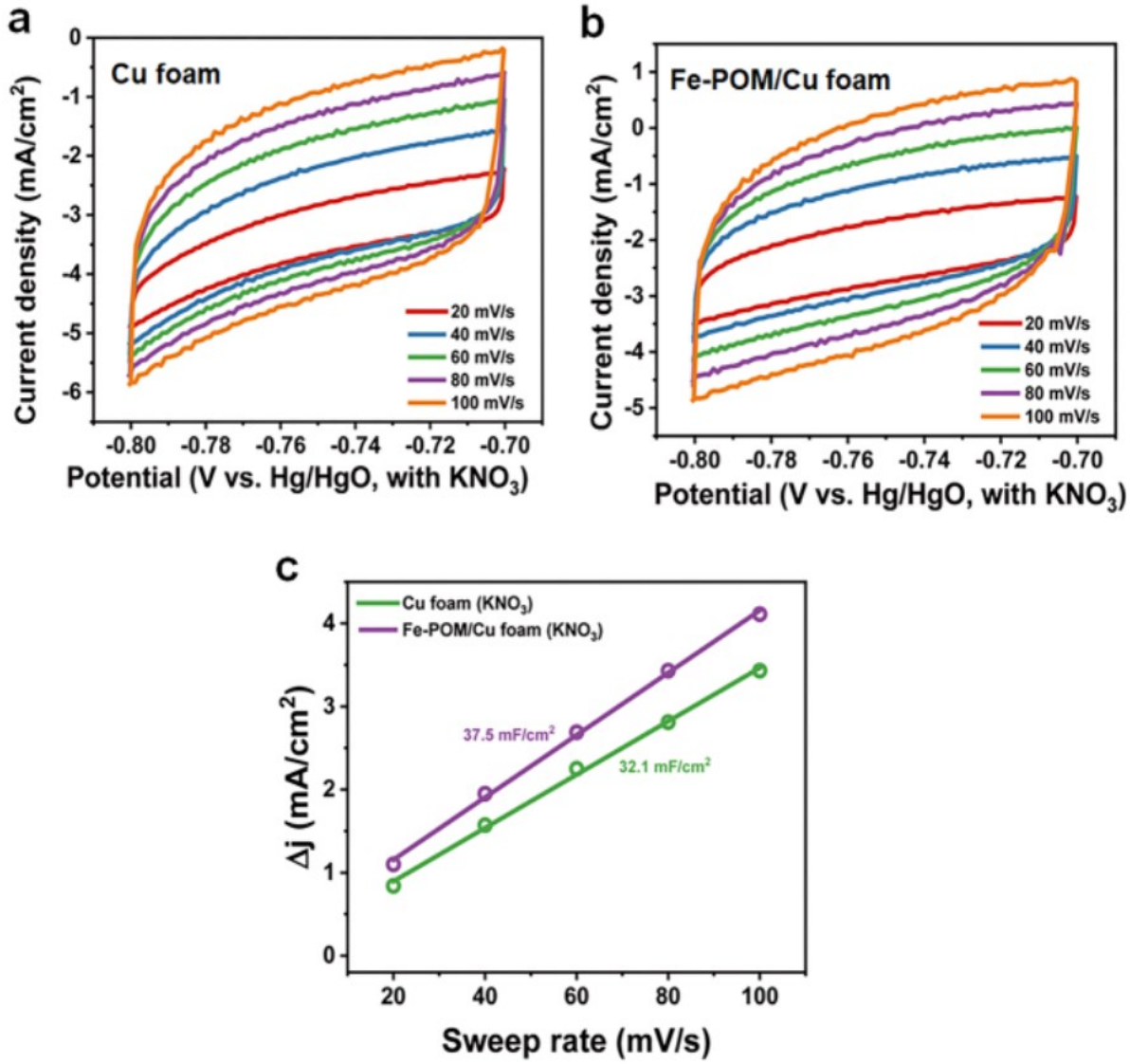

Figure S14. CV plots and calculated double layer capacitance (C_{dl}) values. CV plots for (a) bare Cu foam and (b) Fe-POM/Cu with various scan rates of 20, 40, 60, 80 and 100 mV/s. 1M KOH + 500 ppm KNO_3 solution was used as an electrolyte. (c) C_{dl} values for Cu foam and Fe-POM/Cu.

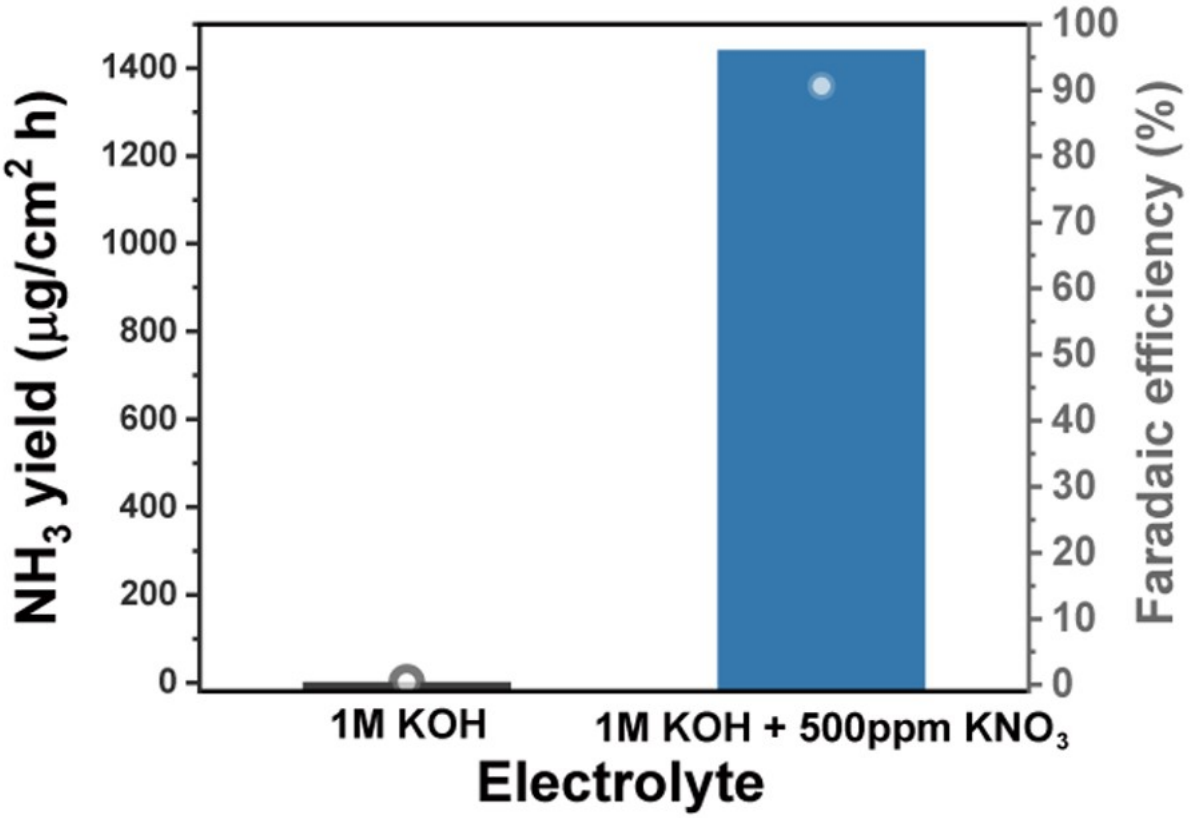

Figure S15. NH_3 yields and faradaic efficiencies with and without NO_3^- feedstock for Fe-POM/Cu electrode.

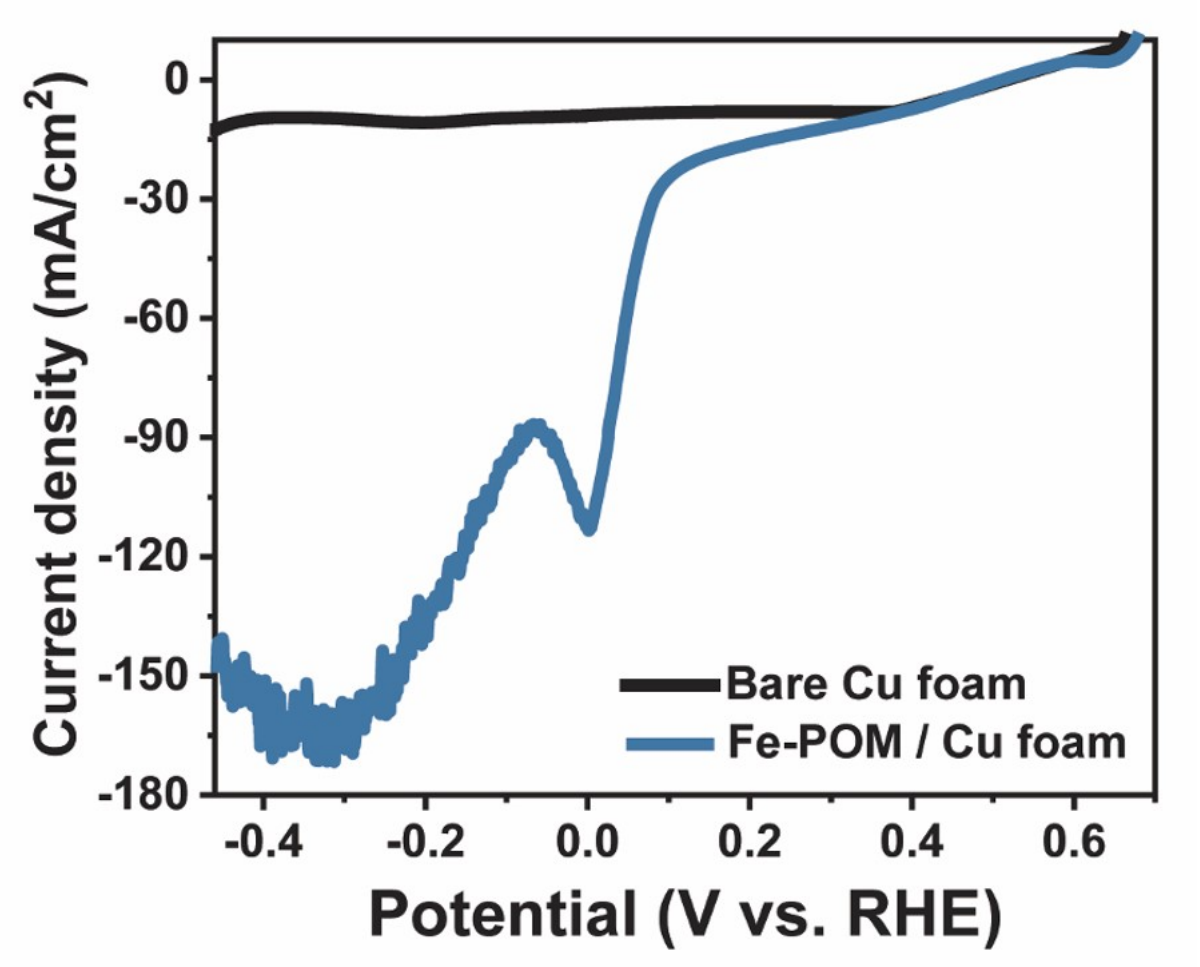

Figure S16. Linear sweep voltammetry (LSV) measurement with scan rate of 5 mV/s.

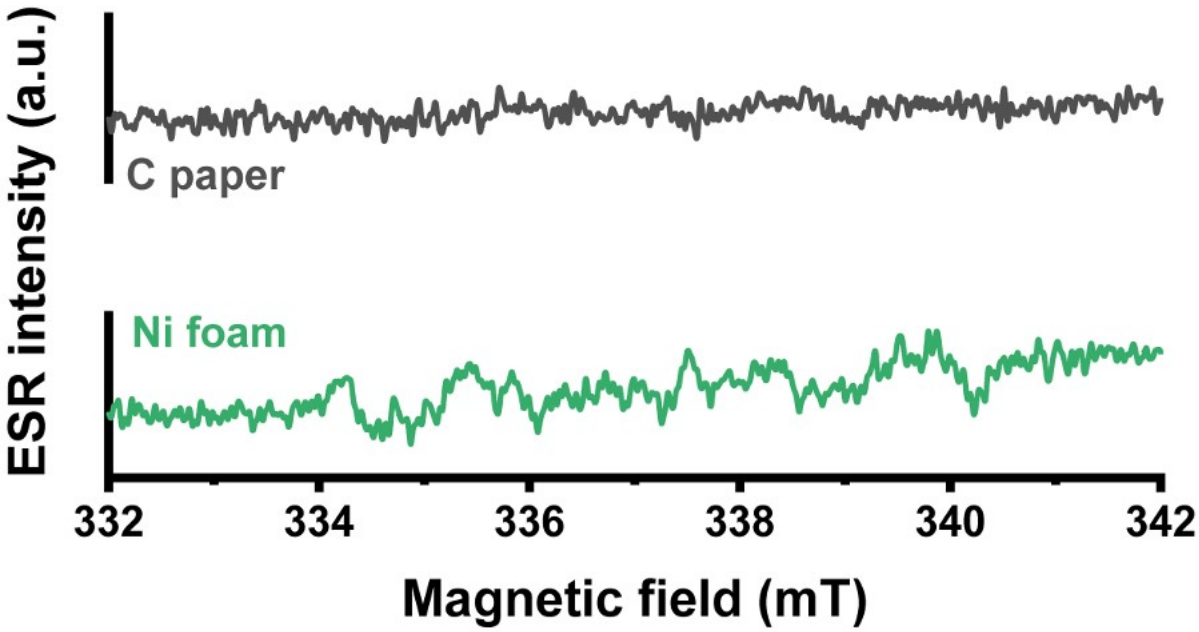

Figure S17. Electron spin resonance (ESR) spectra of the captured solution with DMPO during electrochemical reaction on Ni foam and carbon paper.

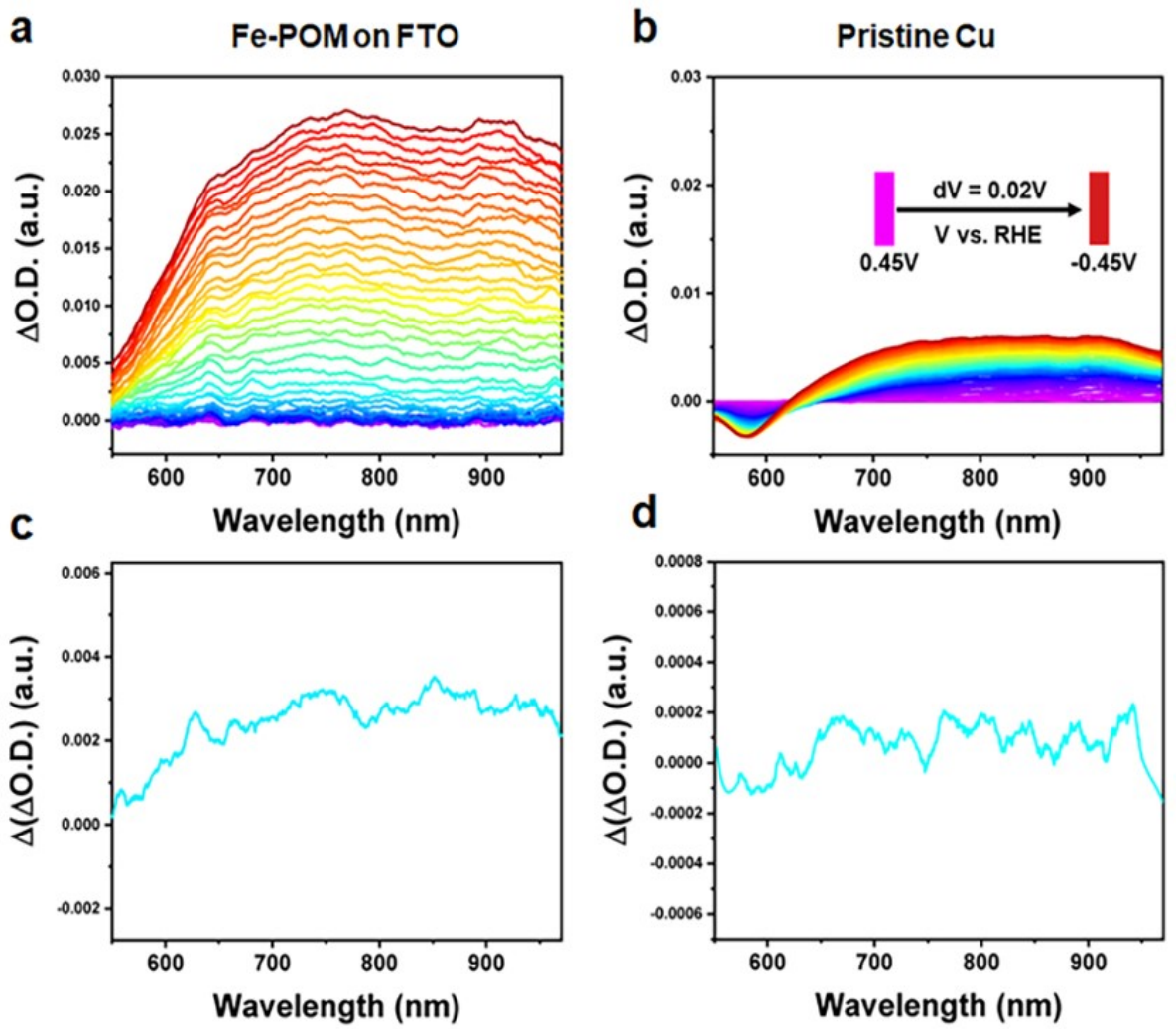

Figure S18. ***Operando*** **spectroelectrochemical analysis.** (a-b) Spectroelectrochemical data and (c-d) redox transition components for Fe-POM on FTO and pristine Cu.

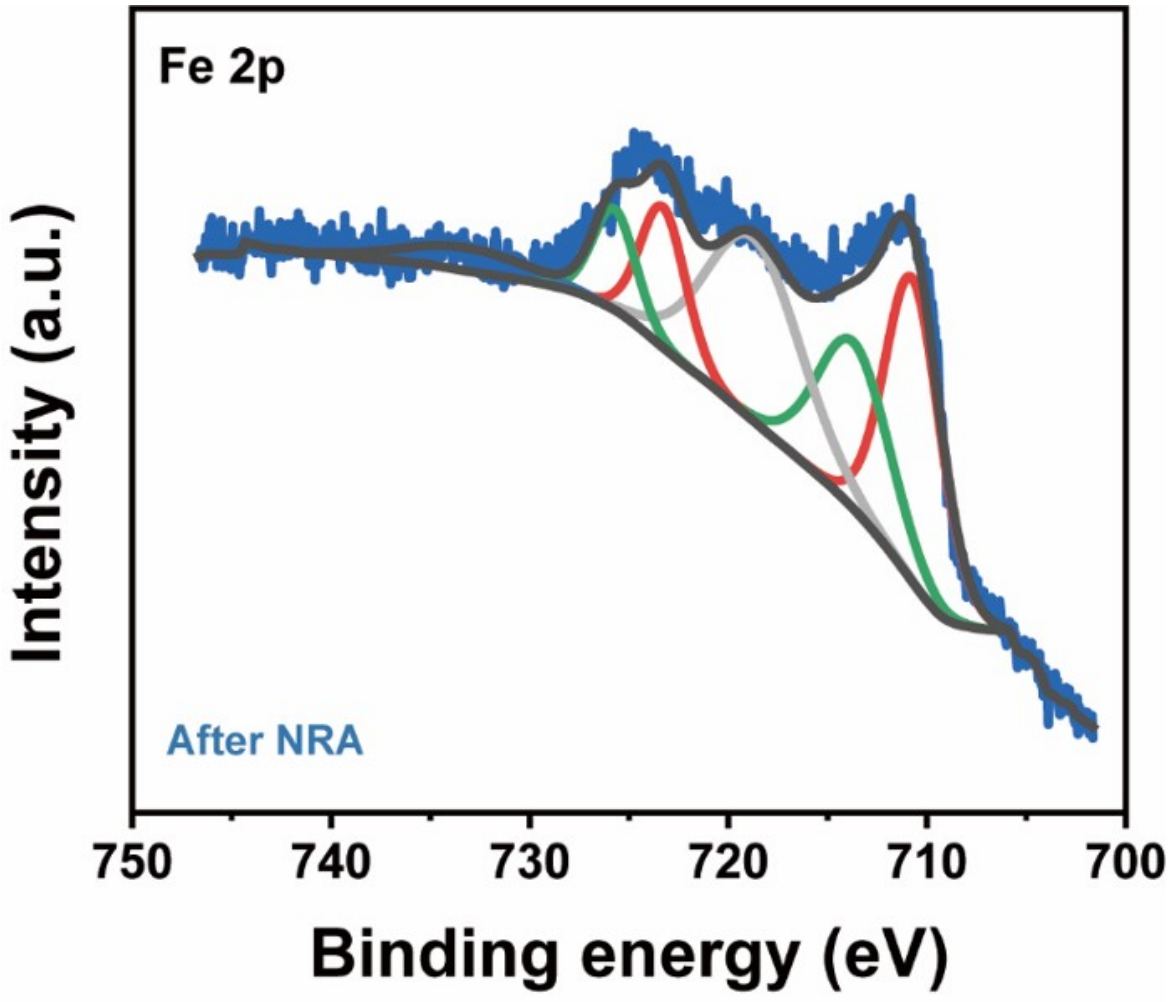

Figure S19. Fe 2p XPS curve for Fe-POM/Cu electrode after electrochemical nitrate reduction for an hour at -0.2 V vs RHE in in 1 M KOH + 500 ppm KNO_3.

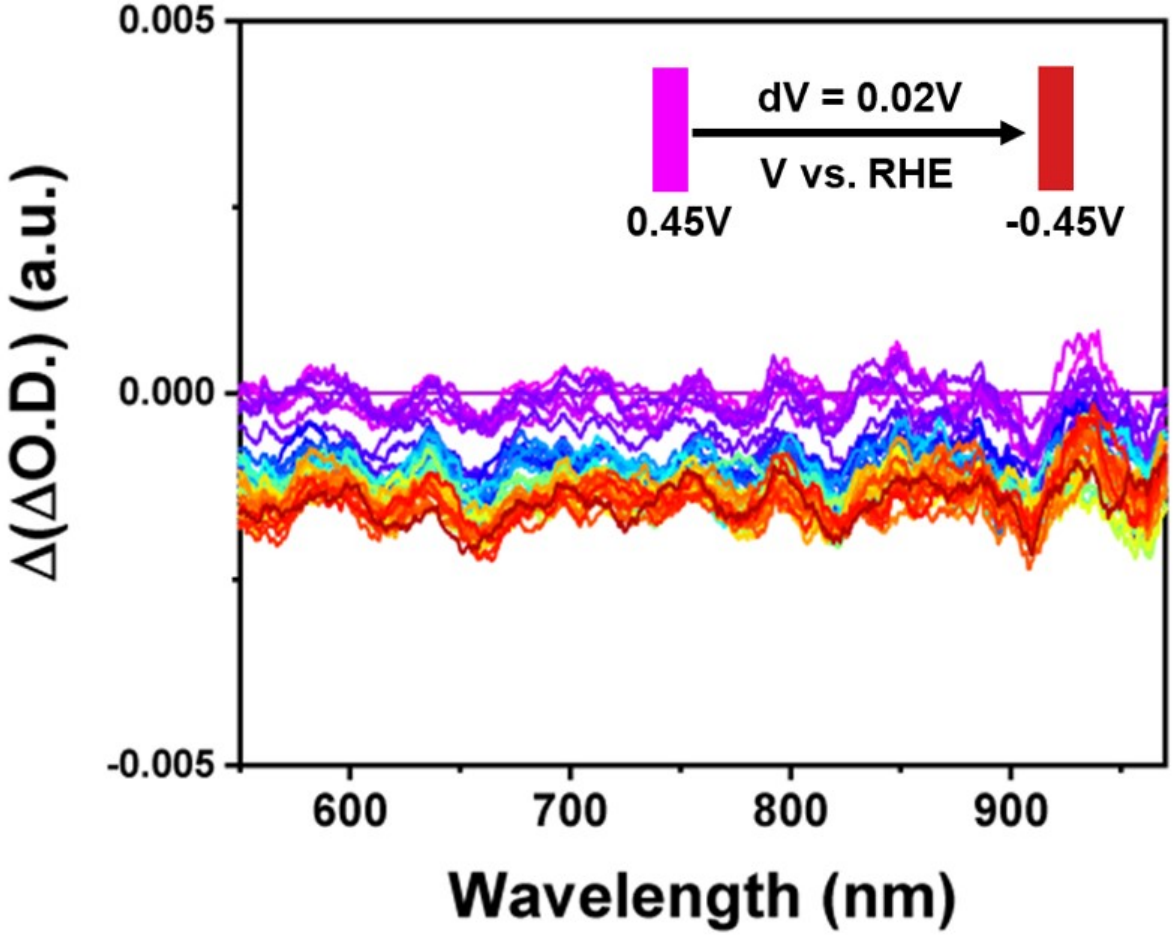

Figure S20. ***Operando*** **spectroelectrochemical data for bare FTO.**

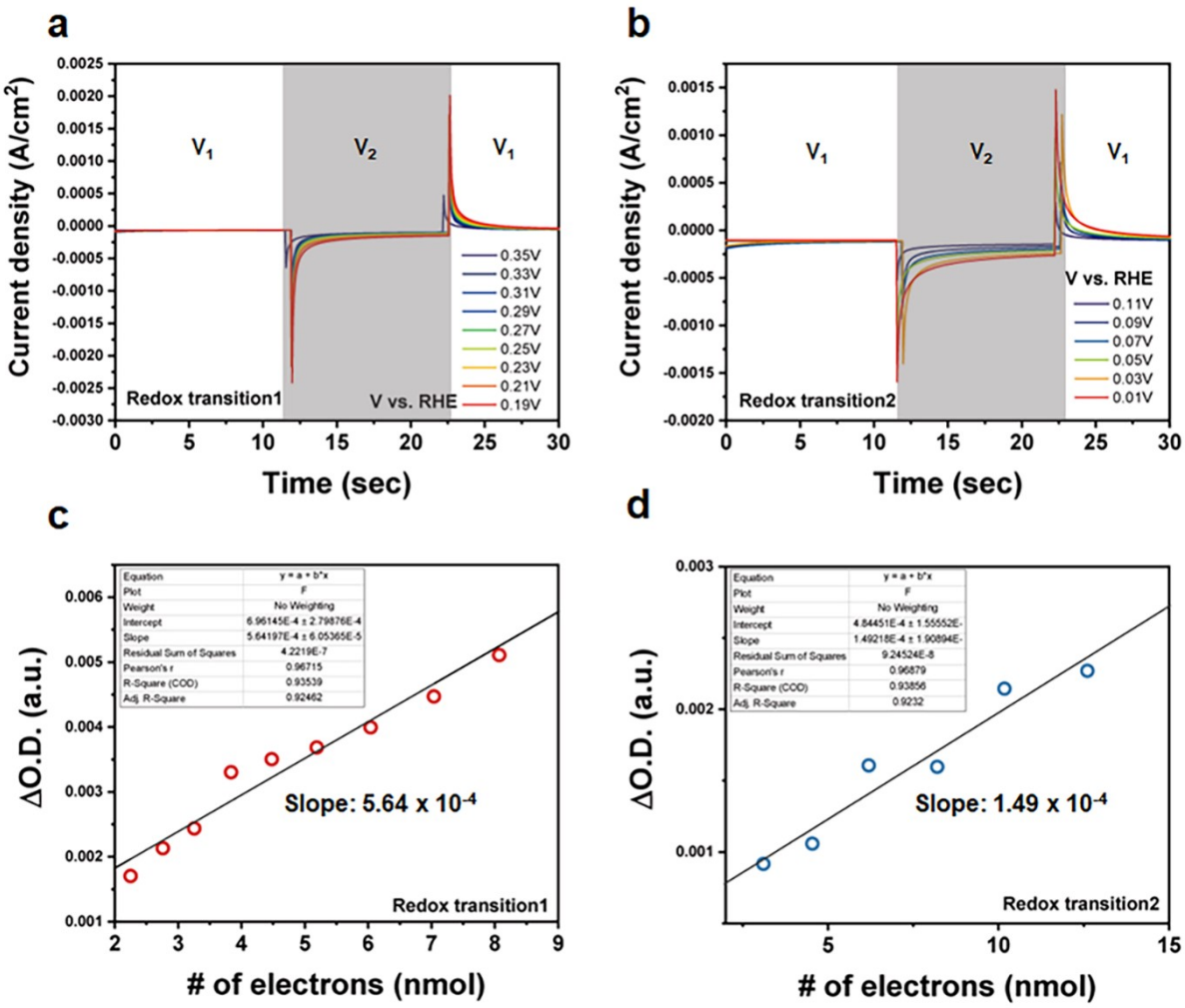

Figure S21. Step potential-spectroelectrochemical analysis. (a-b) Chronoamperometry measurement with step potentials. (c-d) Extinction coefficient for each redox transition plotting the maximum optical signal change with the charge amount from the step potential measurement.

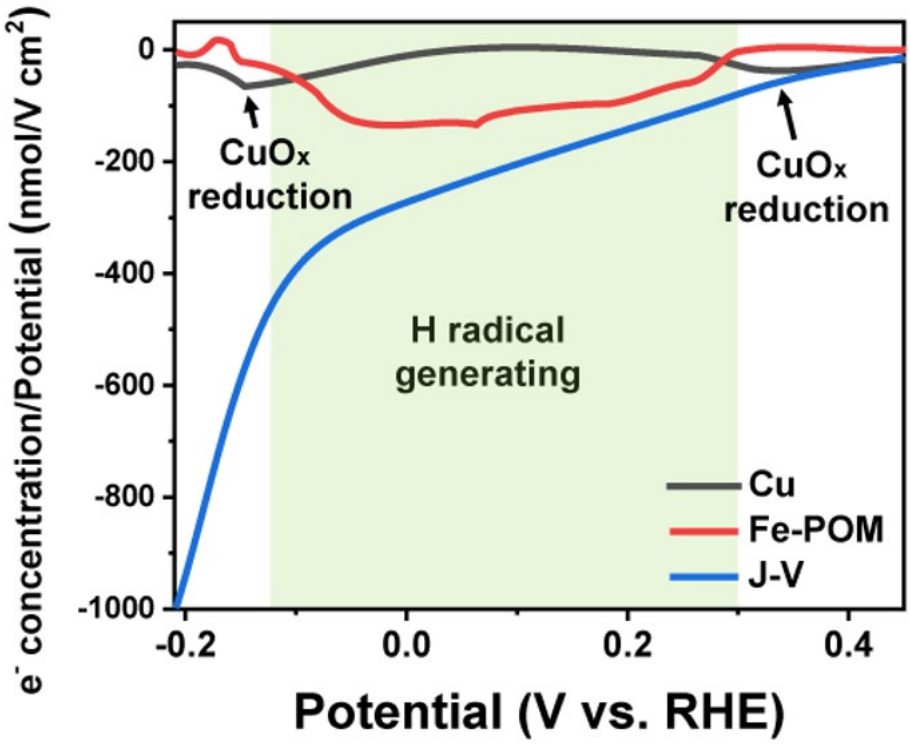

Figure S22. Electron population change of each redox transition at an applied potential and actual current density divided by the faradaic constant and the scan rate.

To correlate the changes in population of each redox state with the observed current density, we differentiate the population change by the applied potential. The observed current density-potential curves were also divided by the faradaic constant and the scan rate to unify the unit (nmol/V cm^2). From the fitted redox transitions corresponding to the potential-dependent optical absorption data, it is evident that the redox transition of Fe cations in Fe-POM appears from 0.25 V vs. RHE.

Table S1. Calculated NH_3 yields and faradaic efficiencies of bare Cu foam and Fe-POM/Cu foam with various applied potentials of 0, -0.1, -0.2, -0.3 and -0.4 V vs. RHE in 1 M KOH + 500 ppm KNO_3.

1M KOH + 500ppm KNO_3	Potential (V vs. RHE)	NH_3 yield ($\mu g/cm^2$ h)	Faradaic efficiency (%)
Fe-POM	0V	89.08	11.16
	-0.1V	416.35	44.19
	-0.2V	1437.44	97.09
	-0.3V	1380.34	86.22
	-0.4V	1383.16	76.05
Cu foam	0V	11.02	4.04
	-0.1V	25.16	6.76
	-0.2V	40.74	10.45
	-0.3V	110.65	23.91
	-0.4V	222.24	26.94

Table S2. Calculated NH_3 yields and faradaic efficiencies of bare Cu foam and Fe-POM/Cu foam with various applied potentials of 0, -0.1, -0.2, -0.3 and -0.4 V vs. RHE in 1 M KOH + 1000 ppm KNO_3.

1M KOH + 1000ppm KNO_3	Potential (V vs. RHE)	NH_3 yield ($\mu g/cm^2$ h)	Faradaic efficiency (%)
Fe-POM	0V	225.05	21.72
	-0.1V	1967.36	85.04
	-0.2V	2806.64	98.96
	-0.3V	2833.83	91.54
	-0.4V	2824.46	89.01

Table S3. Performances of previous works and this work for nitrate reduction to ammonia.

Materials	Potential	FE(%)	NO_3 conc.	Ref no.
Cu/Cu_2O NWA	-0.85 V vs. RHE	81.20 %	200 ppm	1
O-Cu-PTCDA	-0.4 V vs. RHE	77.00 %	500 ppm	2
TiO_{2-x}	-1.6 V vs. SCE	85 %	360 ppm	3
O-SiNW/Au	0.1 V vs. RHE	85.60 %	1000 ppm	4
Fe doped Cu	-0.74 V vs. RHE	86.80 %	200 ppm	5
$Pd\text{-}Cu_2O$	-1.3 V vs. SCE	96 %	50 ppm	6
$10Cu/TiO_{2-x}$	-0.75 V vs. RHE	73.56 %	200 ppm	7
Fe/Ni_2P	-0.4 V vs. RHE	94.30 %	5000 ppm	8
Ru-Cu NW	-0.13 V vs. RHE	93 %	2000 ppm	9
Pd-NDs/Zr-MOF	-1.3 V vs. RHE	58.10 %	500 ppm	10
Fe-POM/Cu	-0.2 V vs. RHE	97.09 % (98.96 %)	500 ppm (1000 ppm)	This work

Table S4. Electrochemical impedance spectroscopy (EIS) fitting data for pristine Cu foam and Fe-POM/Cu foam.

(Ohm)	R1	R2	R3	Equivalent circuit
Cu foam	1.059	10.340	n/a	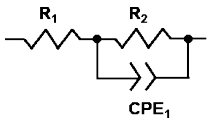
Fe-POM/Cu foam	0.917	1.467	1.121	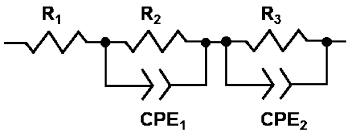

Supporting references

1. Y. Wang, W. Zhou, R. Jia, Y. Yu, B. Zhang, *Angew. Chemie - Int. Ed.* 2020, ***59***, 5350.

2. G. F. Chen, Y. Yuan, H. Jiang, S. Y. Ren, L. X. Ding, L. Ma, T. Wu, J. Lu, H. Wang, *Nat. Energy* 2020, ***5***, 605.

3. R. Jia, Y. Wang, C. Wang, Y. Ling, Y. Yu, B. Zhang, *ACS Catal.* 2020, ***10***, 3533.

4. H. E. Kim, J. Kim, E. C. Ra, H. Zhang, Y. J. Jang, J. S. Lee, *Angew. Chemie - Int. Ed.* 2022, ***61***, 7036.

5. C. Wang, Z. Liu, T. Hu, J. Li, L. Dong, F. Du, C. Li, C. Guo, *ChemSusChem* 2021, ***14*****,** 1825.

6. Y. Xu, K. Ren, T. Ren, M. Wang, Z. Wang, X. Li, L. Wang, H. Wang, *Appl. Catal. B Environ.* 2022, ***306***, 121094.

7. X. Zhang, C. Wang, Y. Guo, B. Zhang, Y. Wang, Y. Yu, *J. Mater. Chem. A* 2022, ***10***, 6448.

8. R. Zhang, Y. Guo, S. Zhang, D. Chen, Y. Zhao, Z. Huang, L. Ma, P. Li, Q. Yang, G. Liang, C. Zhi, *Adv. Energy Mater.* 2022, ***12***, 1.

9. F. Y. Chen, Z. Y. Wu, S. Gupta, D. J. Rivera, S. V Lambeets, S. Pecaut, J. Y. T. Kim, P. Zhu, Y. Z. Finfrock, D. M. Meira, G. King, G. Gao, W. Xu, D. A. Cullen, H. Zhou, Y. Han, D. E. Perea, C. L. Muhich, H. Wang, *Nat. Nanotechnol.* 2022, **17**, 759.

10. M. Jiang, J. Su, X. Song, P. Zhang, M. Zhu, L. Qin, Z. Tie, J. L. Zuo, Z. Jin, *Nano Lett.* 2022, ***22***, 2529.